Renewable and Sustainable Energy Reviews 41 (2015) 1205–1216

Contents lists available at ScienceDirect

Renewable and Sustainable Energy Reviews

journal homepage: www.elsevier.com/locate/rser

Novel nano-structured for the improvement of photo-catalyzed hydrogen production via water splitting with in-situ nano-carbon formation

Ahmed M.A. El Naggar, Heba M. Gobara, Ibrahim M. Nassar *

Egyptian Petroleum Research Institute (EPRI), 1 Ahmed El-Zomor Street, Nasr City, 11727 Cairo, Egypt

ARTICLE INFO

Article history:
Received 19 January 2014
Received in revised form
5 August 2014
Accepted 1 September 2014

Keywords:
II–VI semiconductors nanomaterials
Perovskite
Mixed metal oxides
H_2 production
Electron–hole bear effect
Nano-carbon

ABSTRACT

Photocatalytic water splitting is a promising process for producing H_2 from two abundant renewable sources, namely, water and solar light, with the aid of suitable photocatalysts. In a previous research study, the team of this work succeeded in enhancing the production of H_2 during the water splitting using synthesized Chalcogenide photocatalytic nanoparticles of d-group elements based semiconductors (ZnO and CdS) via a photochemical reaction under UV-light in the presence of methanol as a hole-scavenger. In the current work, a new nano-structured mixed oxide based material in a Perovskite structure is introduced as a novel semiconductor for the water splitting application. The combination of the aforementioned semiconductors and Perovskite in order to improve the photocatalytic activity for an enhanced hydrogen production through water splitting process under visible light irradiation (sunlight) is also discussed through this study. Unpredictable results based on the utilization of Perovskite individually or combined with the other semiconductors were obtained. Hydrogen was aggrandized (since a pioneering and unexpected hydrogen yield was obtained) accompanied with the formation of carbon-species which disclose an innovative reaction mechanism through this research. These results were emphasized by different tools analysis, namely Raman microscopy, SEM, TEM, and surface area. The results obtained in this work reveal that the nano-structured semiconductor/Perovskite system introduced through this work is a promising candidate in the field of hydrogen production with a simultaneous carbon based materials formation.

Contents

* Corresponding author. Tel.: +20 2 227 45902; fax: +20 2 227 727433.
E-mail address: inassar_76@yahoo.com (I.M. Nassar).

http://dx.doi.org/10.1016/j.rser.2014.09.001
1364-0321/

1. Introduction

An important process for future energy supplies is 'photo-hydrogen' production from water splitting; the photocatalytic processes are clean and employ a renewable source as reported for various systems [1–3]. The band gap of a semiconductor should be larger than 1.23 eV, corresponding to the water splitting potential, where the conduction and valence band levels should satisfy the energy requirements to match the reduction and oxidation potentials of H_2O, respectively [4]. Several semiconductor oxides such as TiO_2, ZrO_2, $NbTaO_3$, and $NaTaO_3$, including transition metal oxides, have been studied [5–7]; also the design of nanocomposite nanomaterials has attracted attention due to their high response in UV–visible region for photocatalytic reactions [8,9].

Titanium dioxide (TiO_2) is considered as the best photocatalyst. However, the use of TiO_2 as photocatalysts for water splitting is limited by its redox potential with reference to the normal hydrogen electrode (NHE) [10]. Important studies have been made to improve the photocatalytic activity of titanium dioxide for the water splitting reaction. Modified titanium dioxide was prepared by doping with Fe, Zn, Cu, V, Mg, Be and Ni [11], or by impregnating TiO_2 with noble metals such as Pt, Pd, Ir, Rh and Ru [12]. In particular, the preparation of mixed oxides like CuO, ZnO, NiO and CeO [13–17] has attracted attention for researchers because of the low-cost materials and as they show important photocatalytic properties. The incorporated oxide effect has been related to oxygen vacancies in its crystal structure [18,19].

In a previous work by the authors of this study [20], the photoelectrochemical water splitting for hydrogen production from water–methanol mixture decomposition using either ZnO with energy band gap of 3.37 eV or CdS with energy band gap of 2.42 eV separately or combined together was demonstrated. It is clearly reported that CdS and ZnO have reasonable photocatalytic activity for hydrogen production from water, in the presence of methanol as the hole scavenger, under UV and visible light. A colloidal CdS/ZnO composite system with small particles size (less than 10 nm for each component) was introduced. The CdS electrons homo-generated during its band gap excitation can then be transferred to the conduction band (CB) of ZnO while the holes remain in the CdS particle. This charge separation in a colloidal composite system might help in increasing H_2 production rate especially for those which have particle sizes less than 10 nm. The overall activity of hydrogen production was nearly 6 mmol/h when both semiconductors were physically combined together [20].

The development of new semiconductor based photocatalytic materials is a very challenging task; it involves different deciding factors such as the band gap, carrier transport, catalytic activity, surface related absorption properties and chemical stability [21]. Searches for alternateing photocatalysts are carried out to develop materials that are capable of absorbing visible light, which constitutes a larger portion of the solar light.

One approach that has been studied is to modify the band gap as well as to discover new photocatalysts for identification of new materials with appropriate band gaps. Many mixed metal oxides with early transition metal ions having d^0 configuration (Ti^{4+}, Nb^{5+}, Ta^{5+}) have been explored, specifically several layered Perovskitess, such as $K_2La_2Ti_3O_{10}$, $RbPb_2Nb_3O_{10}$, and $KLaNb_2O_7$, identified as photocatalysts in the presence of co-catalysts (Pt, NiO, etc.) for the evolution of H_2 from water under UV light radiation [22].

These oxides are attractive photocatalytic materials for the following reasons. (1) Their structures consist of two-dimensional Perovskite slabs interleaved with cations, which is expected to increase the lifetime of the photo-generated electrons and holes, and thereby increase the efficiency of the materials [23]. (2) The Perovskite slabs normally made up of metals such as Ti, Nb, or Ta have been preferred as photocatalysts under UV irradiation. (3) Numerous low-temperature synthetic possibilities exist [24] to study the influence of cationic and/or anionic substitutions by the appropriate tuning of the band gaps. For the aforementioned reasons the authors of this study were interested to investigate the Perovskite oxide $K_2La_2Ti_3O_{10}$, as part of their ongoing efforts to identify visible light active photocatalysts for water decomposition.

Various kinds of new mixed oxide semiconductor materials which could absorb visible light were synthesized by Arakawa et al. [25]. The first group is Bi_2MNbO_7 ($M=Al^{3+}$, Ga^{3+}, In^{3+}, Y^{3+}, Rare Earth^{3+}) [26] of $A_2B_2O_7$ pyrochlore structure. The second group is $BiMO_4$ ($M=Nb^{5+}$, Ta^{5+}) [27] of stibotantalite structure and the third group is $InMO_4$ ($M=Nb^{5+}$, Ta^{5+}) of wolframite structure. These materials crystallize in different structures; however, they contain the same octahedral TaO_6 and/or NbO_6 in the structures. The band structure of these materials shows that the conduction band is mainly composed of Ta/Nb d-level and the valence band is mainly composed of O 2p level. The band gaps of these materials determined by UV–visible reflectance spectra were between 2.7 and 2.4 eV. Among these materials NiO_x (surface oxidized Ni) or RuO_2 that promoted $InTaO_4$ and $InNbO_4$ photocatalysts, such as $NiO_x/InTaO_4$, $RuO_2/InTaO_4$ and $NiO_x/InNbO_4$, showed photocatalytic activities for pure water splitting under visible light irradiation ($\lambda=420$ nm, 300 W Xe lamp). However, the activities were very low.

Solar energy is one of the most promising renewable energy sources. Therefore, several solar energy conversion technologies were studied for several decades [28]. The thermochemical cycles for hydrogen production with solar energy were proposed since the 1960s [29]. The thermochemical cycles of halogen and sulfur compounds as intermediates are efficient for hydrogen production by water splitting, but a slight release of those compounds can impose serious environmental problems. The thermochemical cycle with the redox pairs of metal oxides is regarded as the simplest, as well as the most environmentally benign. In the redox cycle of metal oxides, solar energy can convert metal oxides into their reduced form, which can be oxidized by water to produce hydrogen [30,31]. The effects of various synthetic conditions of the semiconductor/Perovskite photocatalysts on their physicochemical properties and photocatalytic H_2 production activity were investigated.

The coupling of two or more semiconductors with different energy gaps is useful to achieve effective charge separation. Accordingly, the present research review focuses on the combination of various semiconductors using either LSCF [Perovskite] individually or combined with ZnO or CdS as well as a ternary mixture of LSCF–CdS–ZnO having different band energies in order to enhance the photocatalytic activity toward water splitting.

The characterization of the catalysts has been done by nitrogen adsorption and TGA–DSC analysis. The morphology and the texture properties of the prepared semiconductors were examined by SEM and TEM, Raman Spectroscopy analysis and total carbon measurement in order to explore the carbon species formed within their structure. The water splitting reaction has been carried out at room temperature using a water–methanol mixture under visible light radiation.

2. Experimental

2.1. Materials

Three different semiconductors, namely cadmium sulfide (CdS), zinc oxide (ZnO) and mixed oxides of lanthanum, strontium, cobalt and iron as a combined mixture in the following formula ($La_{0.6}Sr_{0.4}Co_{0.2}Fe_{0.8}O_3$), which is known as the Perovskite structure, are utilized through this study for the hydrogen production purpose.

Perovskite [oxygen selective material]: A Perovskite structure is any material with the same type of crystal structure as that of calcium titanium oxide ($CaTiO_3$), known as the Perovskite structure, with the oxygen in the face centers. The Perovskite structure is adopted by many oxides that have the chemical formula ABO_3, where ‘A’ and ‘B’ are two cations of very different sizes, and X is an anion (always oxygen) that bonds to both. The ‘A’ atoms are larger than the ‘B’ atoms where A is a mono- or divalent metal (a larger metal cation, such as Ca^{2+}) and B is a tetra- or pentavalent metal (a smaller metal cation, such as Ti^{4+}). As outlined in Fig. 1, the A atoms form the corners of the ‘cubic’ cells, B atoms are in the center and the oxygen atoms are situated in the faces' centers.

The ideal cubic-symmetry structure has the B cation in 6-fold coordination, surrounded by an octahedron of anions, and the A cation in 12-fold cub-octahedral coordination. The relative ion size requirements for stability of the cubic structure are quite stringent so slight buckling and distortion can produce several lower-symmetry distorted versions, in which the coordination numbers of A cations, B cations or both are reduced.

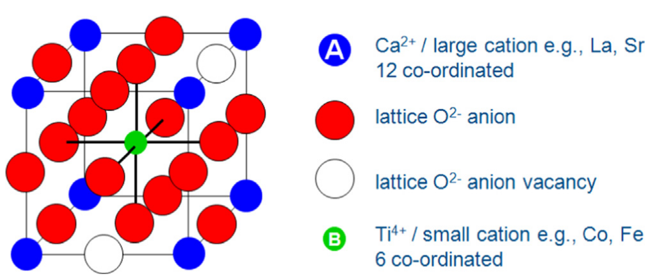

Fig. 1. Diagrammatic structure of Perovskite cubic lattice.

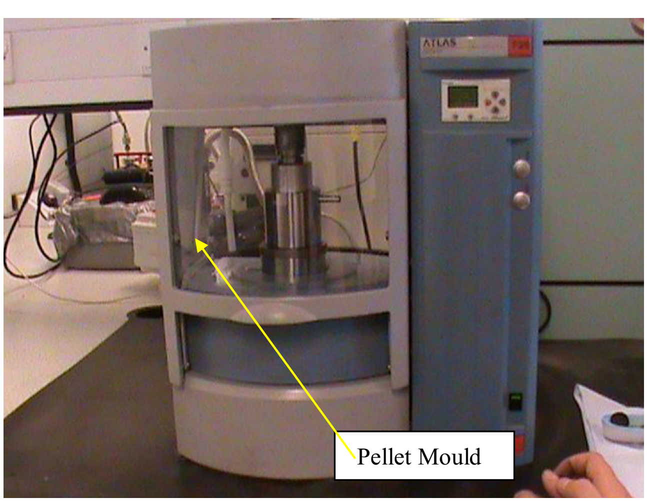

Fig. 2. Oxygen pellet disc production via press machine.

2.2. Preparation of semiconductors nanoparticles

Synthesis, evaluation and identification of CdS and ZnO nanoparticles were described elsewhere by Nassar et al. [32] and El Naggar et al. [20] respectively, while the typical synthesis of LSCF oxide nanoparticles is as follows. At the beginning a solution of La, Sr, Co and Fe ions with the molar ratios of Perovskite previously given in Section 2.1, with a total metal ion concentration of 1 M was prepared at 60 °C. All the precursors of the metals used during the metal solution preparation were metal nitrate hexahydrate and purchased from Sigma-Aldrich UK. Simultaneously, 1 M solution of the precipitating agent was prepared and then heated to a certain temperature of 60 °C. The metals nitrate solution was afterward added at once to the precipitating agent at vigorous stirring of 750 rpm and kept for a reaction time of 3 h. After the reaction was complete, a black precipitate was deposited in the bottom of the reaction holding flask. The precipitate was then collected and washed several times with absolute ethanol and distilled water. Finally, the mixed oxide sample was obtained by centrifugation and dehydration of the precipitate in vacuum at 120 °C overnight [33,34].

In order to produce a non-porous layer (dense film) as oxygen scavenger within the structure of LSCF oxide, the obtained powder after drying was compacted in a pellet disc shape under pressure using a hydraulic machine. The press machine shown in Fig. 2 was used to prepare the pellet discs applying pressure of 5 t at ambient temperature. For Perovskite discs production 4 g of metal oxides mixture powder was sandwiched between two mirrored surfaces of stainless steel dies, which was then accommodated inside a pellet die mould and finally pressed.

The three types of pellets prepared were then subjected to the sintering process at temperature of 1200 °C, with a ramping rate of 1 °C/min and dwell time of 12 h, in order to produce a dense film. Cooling was then done over a period of $\sim$12 h to avoid any structural damage that might take place due to fast cooling [35,36].

2.3. LSCF nanoparticles characterizations

The texture properties and morphology of the prepared LSCF nanoparticles as a semiconductor were examined using a scanning electron microscope (SEM). The semiconductors samples after the splitting application were then subjected to transmission electron microscopy (TEM), Raman Spectroscopy analysis and total carbon measurement in order to explore the carbon species formed within their structure. Before subjecting to the microscope, all samples were sonicated into ethanol for 10 min in order to get homogenous dispersed particles. The nanoparticles surface area, average pore size and pores distributions were also determined using a BET surface area analyzer. Finally the semiconductor thermal stability was also measured using a TGA–DSC equipment.

2.3.1. Analytical techniques

2.3.1.1. Scanning electron microscope (SEM). The model of SEM used to analyze the morphology of the prepared oxygen selective semiconductor in this study is the XL30 ESEM. The ESEM offers high secondary electron imaging at high pressure (as high as 10 Torr) and high temperature (as high as 1000 °C).

This means the samples can be examined in their natural state without significant sample modification or preparation.

2.3.1.2. Transmission electron microscopy (TEM). The scanning electron microscope used in the present work is a high-resolution Electron Microscopy model JEM 2100 (JEOL, Japan). It offers high-resolution electron imaging up to 0.143 nm and as high as 1.5 million times magnification.

2.3.1.3. BET surface area analysis. The prepared oxide form bi-metallic nano-catalyst was characterized by nitrogen adsorption–desorption isotherms at $-196\ ^{\circ}C$ using a NOVA 3200 apparatus, USA. The samples were pre-treated under vacuum (10^{-4} Torr) at $300\ ^{\circ}C$ for 24 h. Surface areas (S_{BET}) were calculated from the adsorption branch of the isotherms by applying BET equation. Particle size distribution was in the end calculated using the Barrett, Joyner and Halenda (BJH) method from desorption branch of the isotherms.

2.3.1.4. TGA and DSC analysis. Thermal Gravimetric Analysis and Differential Scanning Calorimetry [DSC–TGA] analyses were carried out for the metal oxide samples using simultaneous DSC–TGA, model (SDTQ 600, USA) under N_2 atmosphere, with a heating rate of $10\ ^{\circ}C\ min^{-1}$.

2.3.1.5. Gas chromatography (GC). The collected gas after the water splitting process was analyzed using a gas chromatography instrument manufactured by PerkinElmer-USA, equipped with a thermal conductivity detector (TCD) and gas analyzer to indentify the collected gas components.

2.4. Hydrogen production system

The hydrogen evolution experiments are carried out using a photo-catalytic reaction cell which is formerly displayed in [19]. The hydrogen production procedures were started by preparing the water solution system, which consisted of water and methanol (50:50 wt%), while the semiconductors were then added to the system at a concentration of 0.25 wt% either using binary semiconductors or via combining the three of them together. LSCF was first used alone, then binary mixtures of LSCF with Cd and Zn were used and finally a mixture of the three of them together. The efficiency of the Cd/Zn binary mixture in hydrogen evolution under sunlight was also tested through this study. After the hydrogen system was fully set up as given in [19], the semiconductor/water solution suspension vessel was degassed via a purging process using pure N_2 for about 5 min in order to provide inert atmosphere during the splitting process. This step was necessary in order to avoid the presence of air which in sequence can restrict the water splitting process via providing oxygen owing to the fact that oxygen represents about one-fifth of the air

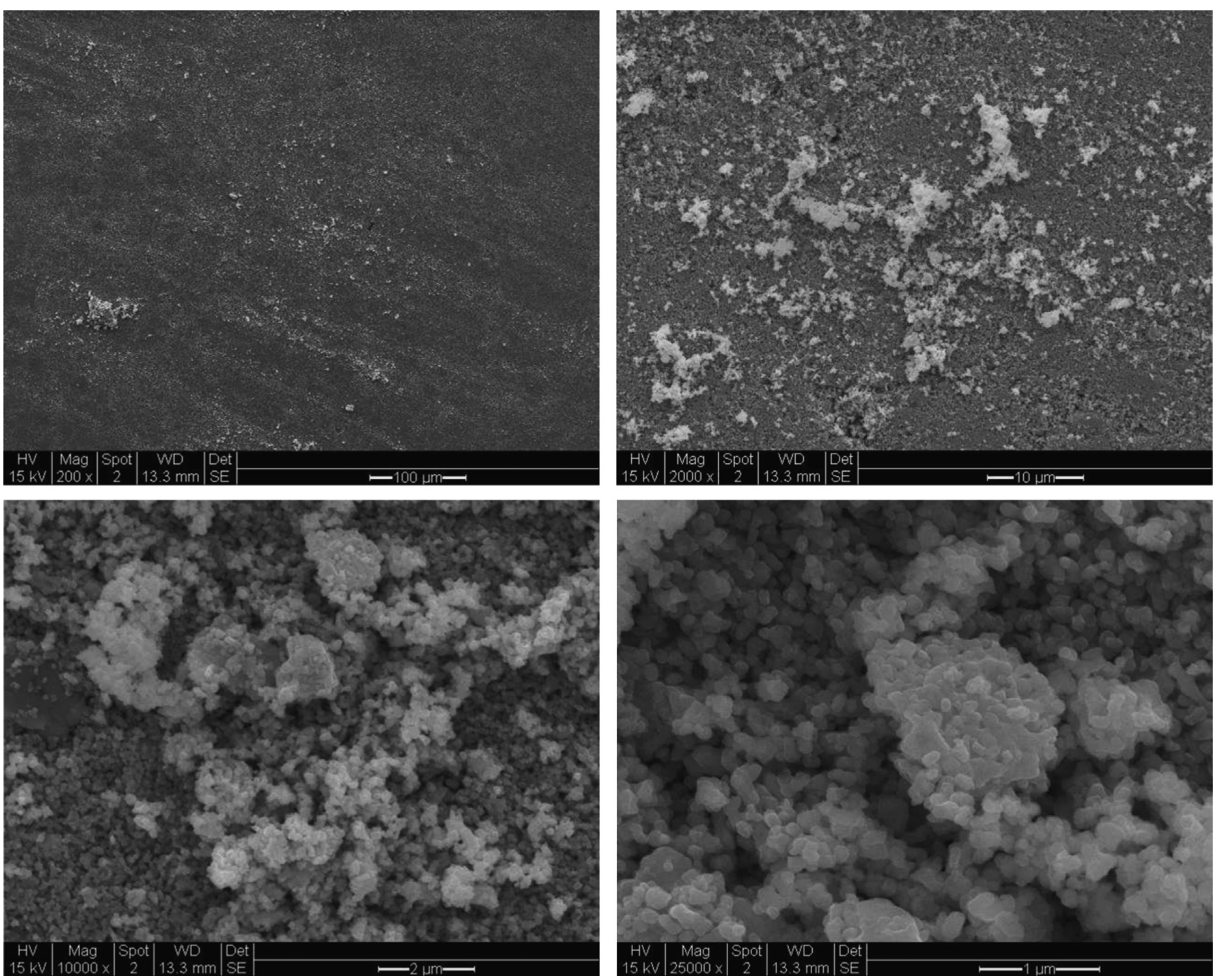

Fig. 3. Perovskite pellet surface structure before sintering at four magnifications.

composition. The water solution was then exposed to the sunlight visible radiation for a period of 72 h of the actual sunlight [12 h/day] under a vigorous stirring of 600 rpm. The gas collected at the end of each experiment was then evaluated by the gas chromatography (GC).

3. Result and discussion

The characterizations of two of the semiconductors that were utilized through this work, namely, CdS and ZnO, were previously discussed in [20,32] as formerly mentioned in the experimental section. Characterization of the other semiconductor, particularly Perovskite structured LSCF oxide, is discussed in the following sections.

3.1. Texture properties

3.1.1. SEM

The obtained powder of metal oxides mixture particles after synthesis, as illustrated in the experimental section, had been pressed together to form pellet disc-shaped materials which were then subjected to sintering at a high temperature of 1200 °C. The structure of the obtained discs, before and after sintering at both pellet surface as well as the cross-section, is shown in Figs. 3–5, and will be discussed below.

At the pellet surface before sintering, as illustrated in Fig. 4, the metal oxide mixture showed a smooth, non-uniform and highly porous structure, as displayed in the SEM images at high magnifications. After sintering at 1200 °C the membrane surface showed radically different morphology, as illustrated in Fig. 4. A smooth, uniform and non-porous surface had been formed after thermal treatment. SEM analysis at high magnifications also showed the formation of a metal oxide mixture layer of particles ranging in size from about 1 μm to a few hundreds nanometers.

At the cross section, as illustrated in the SEM images given in Fig. 5, the Perovskite again showed a morphology different from the one obtained at its surface. Unlike the surface structure, the formation of a uniform, dense layer along the cross section with 'wavy nature' could be detected. The formation of a dense layer along the cross-section is likely to be explained as a result of the higher stress applicable on the inner particles of pellet-shaped Perovskite than on the particles at its surface during the sintering process at high temperature. This high stress has made them highly compressed together, while being softened due to the effect of high temperature. This dense layer formed at the middle part of the LSCF is the reason behind the increased ability for oxygen capture since it provides better selectivity toward oxygen.

3.1.2. Surface area and pores identification

N_2 adsorption–desorption isotherms and surface parameters are carried out to investigate the textural characteristics of

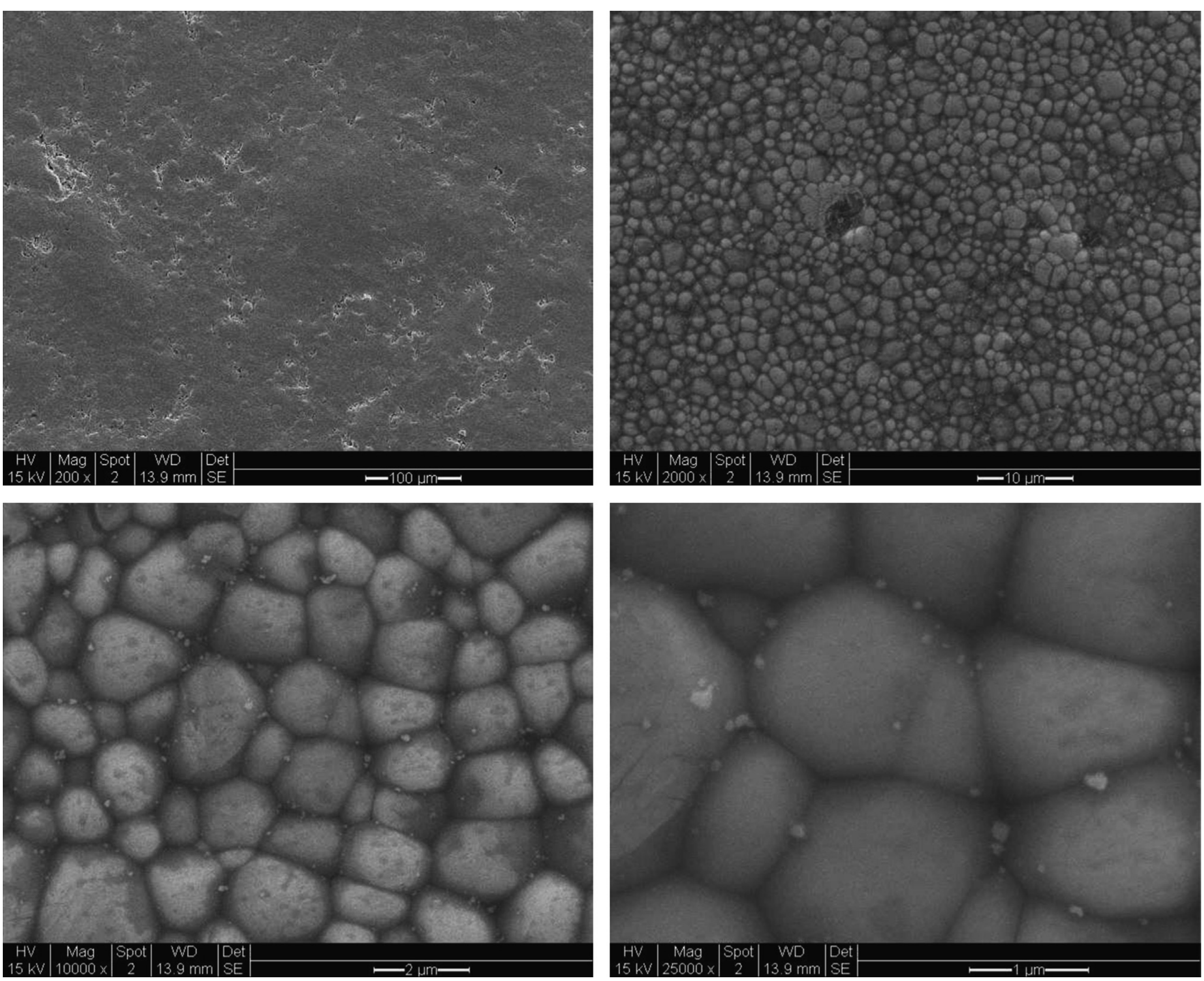

Fig. 4. Pellet non-porous surface structure after sintering at temperature of 1200 °C.

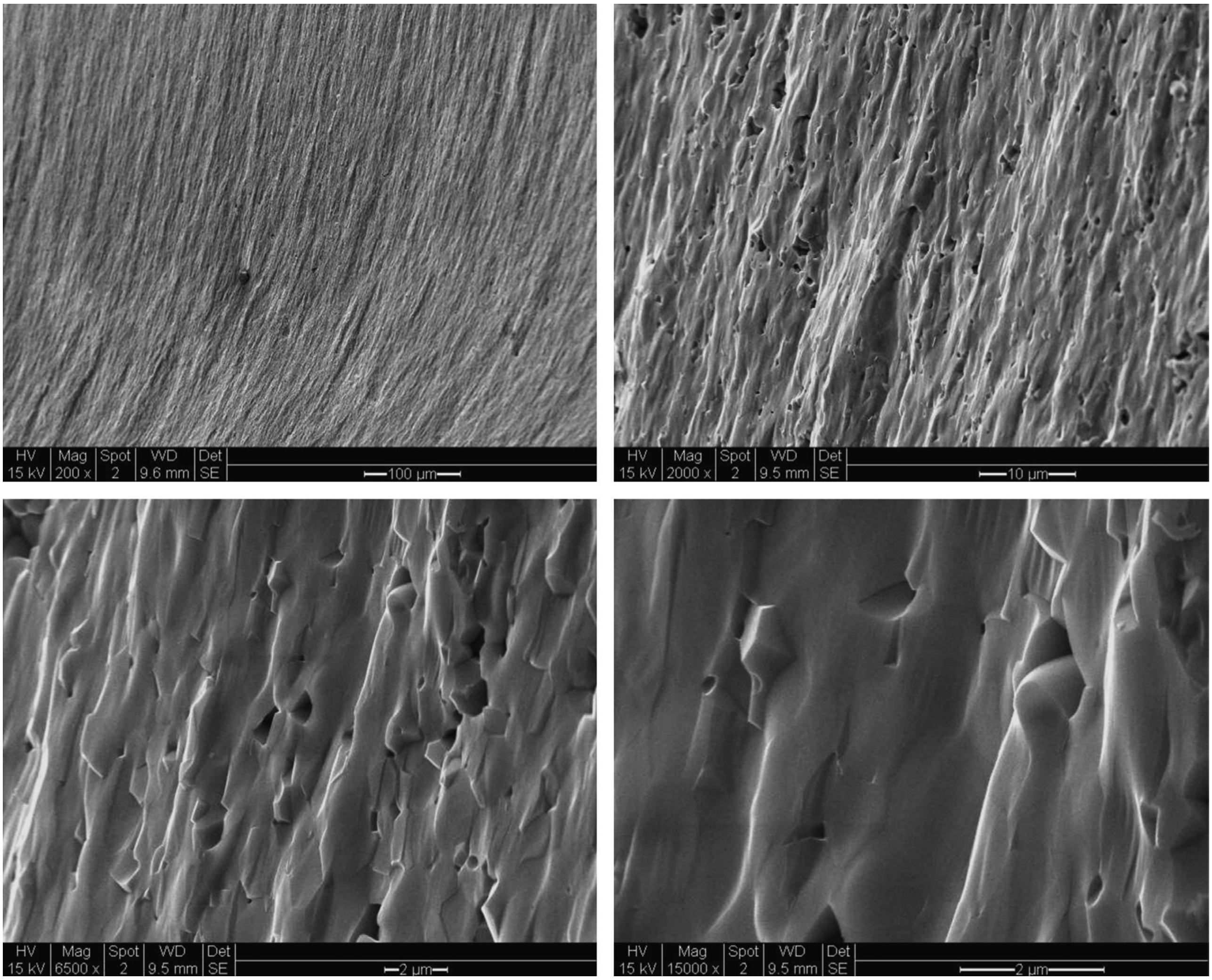

Fig. 5. Dense layer formation at the pellet cross section at four magnifications.

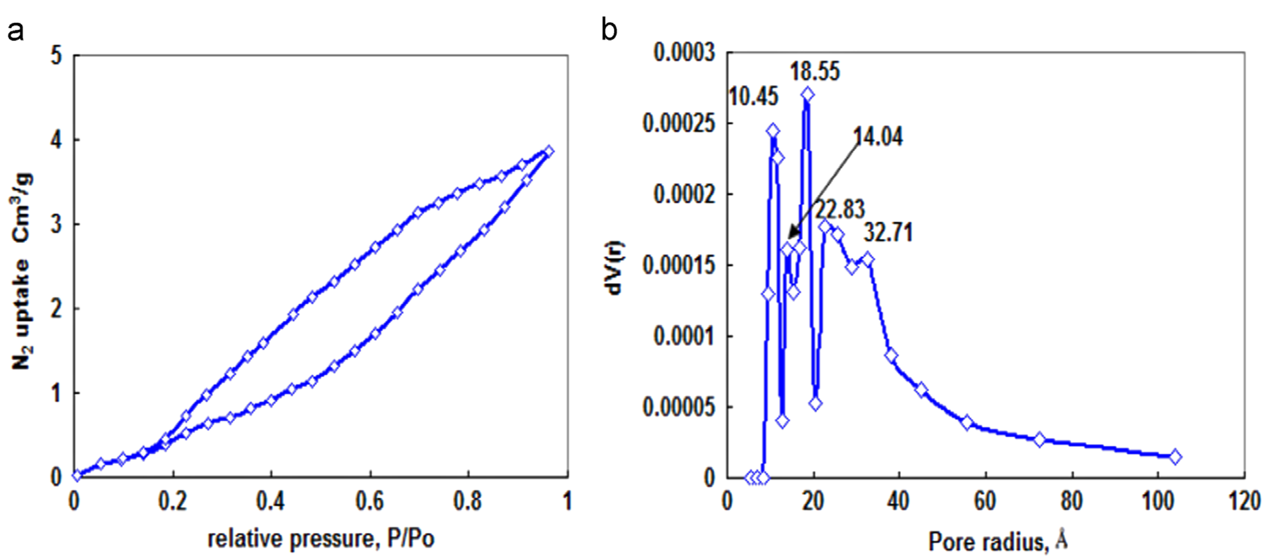

Fig. 6. Perovskite sample: (a) N_2 adsorption-desorption isotherms, (b) pore size distribution curve.

Perovskite. Fig. 6 illustrates N_2 adsorption–desorption isotherms and pore size distribution curves calculated by the BJH method.

The obtained N_2 adsorption–desorption isotherms of the neat Perovskite belongs to type III according to Brunauer and Emmett's classification, associated mainly with weak gas–solid interactions (Fig. 6a). This type of isotherm is related to nonporous or macroporous materials. An almost H3-type hysteresis loop is exhibited over a wide relative pressure range down to $P/P_o \sim 0.2$, being

characteristic of mixed pore systems. This type of loop is usually attributed to non-rigid aggregates or plate-like particles forming slit-shaped pores, including pores in the micropore region [37]. According to the surface area measurements and calculation, the neat perovskite showed a specific surface area of 3.44 m^2/g while the total pore volume and the average pore radius are 0.006 cm^3/g and 3.49 nm respectively. On the other hand the obtained PSD curve (Fig. 6b) indicates the presence of mixed narrow and wide mesopore systems, with pore radii centered at 10.45, 14.04, 18.55, 22.83 and 32.71 Å.

3.2. Thermal analysis

The thermal stability of the prepared LSCF mixed oxide (Perovskite) is discussed through Fig. 7. The LSCF nanoparticles showed high thermal stability in terms of the overall weight loss obtained at the end of this testing time and up to temperature of 800 °C. The oxide showed less than 0.1 wt% weight loss at temperature up to 200 °C while the total weight loss, at the end of test, was 0.7 wt%. TGA analysis was apparently necessary in order to find the semiconductor stability throughout the water splitting process since the process was carried out under sunlight. This is due to the expected huge heat generation within the system as a result of introducing the solar energy as the radiation source.

In line with the TGA analysis, an exothermic peak was detected by the DSC thermogram at a temperature of about 180 °C. This peak might be related to the release of adsorbed water molecules from the surface of mixed oxides nanoparticles.

3.3. Hydrogen production reactivity

It was reported by [38] that the mechanism of the photocatalytic H_2 production is caused by electron–hole pairs in the semiconductors. Hence the differences between energy band gaps for semiconductors have important roles in their influence as a photocatalyst. The hydrogen production results for the semiconductors used through this study are matched with this concept since they are different in band gaps. The semiconductors utilized through this study showed unique activity toward the production of hydrogen via water splitting, as reported in Table 1.

The hydrogen production, according to Table 1, was achieved using either LSCF individually or in a binary combination with CdS or ZnO and in a triple mixture (equal % by weight) of all of them together. According to the data mentioned in Table 1, LSCF showed reasonable activity toward water splitting. However, the coupling between LSCF with either ZnO or CdO led to hydrogen concentrations not achieved

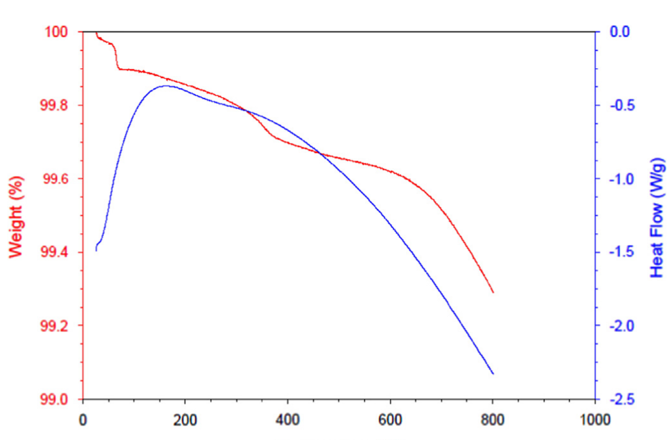

Fig. 7. Perovskited LSCF nanoparticles TGA and DSC analysis.

Table 1
Semiconductors effect on the hydrogen percent and H_2 content in the produced gas.

Semiconductor type	H_2% in the produced gas	H_2 production (mmol/h)
LSCF	99.7	6.35
LSCF–CdS	96.8	24.68
LSCF–ZnO	98.0	28.94
ZnO–CdS	12	4.80
LSCF-CdS-ZnO	97.5	17.97

previously. In comparison to what is given through various studies in literature or even by a previous study done by the authors of this study [20], the highest hydrogen yield reported via these ones was about 6 mmol/h. In this work a unique hydrogen yield, compared to literature, of 6.35 mmol/h was obtained by introducing LSCF alone to the water splitting system. Nevertheless an increase of approximately 4- and 5 folds in the hydrogen production was observed when LSCF was coupled with CdS and ZnO respectively. This can be attributed to the overlapping between the energy levels of the LSCF and the two semiconductors when they were mixed together which in turn led to an improvement in their energy gap. This consequently resulted in developing the semiconductors system photoactivity toward the water splitting into hydrogen. A reverse result in the hydrogen yield was obtained when a mixture of the three semiconductors together was used in the splitting process. This can be explained due to the random interfering of the semiconductors electrons and their energy levels which were reflected accordingly in the hydrogen concentration produced.

3.3.1. Photocatalytic hydrogen production improvement

In comparison to some other research available in the literature, the semiconductors prepared during this study performed very well. Liu et al. [39] developed Au nanoparticle (NP) photosensitization over $SrTiO_3$ semiconductors with a large band gap as a promising strategy for developing visible light responsive photocatalytic materials. In their work, they reported a remarkable visible light photocatalytic water oxidation activity and H_2 production was found to be 14.9 μmol/ h.

Tijare et al. [40] synthesized a visible light-active $BaMnO_x$ type photocatalyst by using a sol–gel method. The photocatalytic hydrogen generation was carried out by using Pt as co-catalyst and ethanol as a sacrificial donor. Hydrogen generation was investigated by ethanol-assisted water splitting reaction under visible light irradiation, using a compact glass reactor and a tungsten lamp as source of visible light. The rate of photocatalytic hydrogen evolution was observed to be 7463 μmol g^{-1} h^{-1} of Pt–$BaMnO_x$ photocatalyst.

Jang et al. [41] successfully synthesized $CaTi_{1-x}Fe_xO_3$ photocatalysts by a solid state reaction method. They found that Fe doping plays an important role in inducing the visible light absorption in $CaTiO_3$, and showed the photocatalytic activity toward hydrogen production in the system of $CaTiO_3$ under visible light irradiation, specifically, the 0.25 wt% Pt loaded on $CaTi_{0.9}Fe_{0.1}O_3$ sample. This semiconductor showed significant H_2 production since a yield of 83 mmole/g was attained. By comparison to the photocatalytic activity of the most active sample in the current work (LSCF–ZnO) higher hydrogen flux, in particular 115.76 mmole/g, is obtained which is apparently higher than that produced by the authors in [40].

Choi et al. [42] demonstrated the photocatalytic production of H_2 from water splitting on $Ni/NiO/KNbO_3/CdS$ nanocomposites using visible light irradiation at wavelengths >400 nm in the presence of isopropanol. The inherent photocatalytic activity of bulk-phase CdS was enhanced by combining Q-sized CdS with

$KNbO_3$ and Ni deposited on $KNbO_3$. The activity enhancement is most likely due to the effective charge separation of photo-generated electrons and holes in CdS that is achieved by electron injection into the conduction band of $KNbO_3$ and the reduced states of niobium (e.g., Nb(IV) and Nb(III)) that in turn can contribute to enhance the reactivity in the $KNbO_3$ composites by mediating an effective electron transfer to bound protons. The authors also observed that the efficient attachment of Q-size CdS and the deposition of nickel on the $KNbO_3$ surface increases H_2 production rates. Other factors that influence the rate of H_2 production, including the nature of the electron donors and the solution pH, were also determined. The Ni/NiO/$KNbO_3$/CdS nano-composite system appears to be a promising candidate for possible practical applications including the production of H_2 under visible light. The highest photocatalytic H_2 production yield achieved under controlled condition (0.1% of Ni and calcinations temperature was 925 °C) seems to be 150 μmol g^{-1} h^{-1}.

Pérez-Larios et al. [43] prepared TiO_2–ZnO mixed oxides photo-conductors by the sol–gel method and used for the H_2 production via water splitting. These solids were proved in the photocatalytic water splitting and were six times more active (1300 μmol/h) than TiO_2 as a reference (190 μmol/h) semiconductor.

Kudo [44] developed various alkali and alkaline earth tantalites as a new group of photocatalyst materials for splitting of water into H_2 and O_2 under UV–visible irradiation. They showed activities even without co-catalysts such as Pt, being different from titanate photocatalysts. NiO co-catalysts were loaded on the tantalate photocatalysts, through which the photocatalytic activities were markedly increased. Among the tantalates, NiO/$NaTaO_3$ doped with La showed the highest activity. Pt/$SrTiO_3$ co-doped with Cr and Sb or Ta photocatalysts showed high activities for H_2 evolution from aqueous solutions containing reducing reagents under visible light irradiation. The maximum photocatalytic hydrogen evolution was found to be 940 μmol/h.

Ye et al. [45] synthesized transition metal-doped $InTaO_4$ and $InNbO_4$. Among these doped materials, Ni-doped $InTaO_4$ and Ni-doped $InNbO_4$ photocatalysts such as $NiO_x/In_{0.9}Ni_{0.1}TaO_4$, $RuO_2/In_{0.9}Ni_{0.1}TaO_4$, $NiO_x/In_{0.9}Ni_{0.1}TaO_4$ and $RuO_2/In_{0.9}Ni_{0.1}TaO_4$ showed the highest activities. The rates of H_2 and O_2 evolution were 16.6 and 8.3 μmol/h, respectively.

In comparison to the above-mentioned results, obtained from literature survey, the semiconductors utilized in this research/review have shown better performance. A hydrogen production of at least four times more than the highest yield reported by the authors above was attained using either LSCF mixed zinc oxide or LSCF mixed cadmium sulfide or the ternary mixture of LSCF–CdS–ZnO. This may be related to the high surface area of the composite system leading to porosity increment as evidenced from PSD curve (c.f. N_2 physisorption section after mixing the composite system). In addition the formation of nano-carbon species, as noticed, during the splitting process might be one of the reasons behind improving the surface activity of the semiconductors toward water splitting. The carbon formation, as next given, is confirmed by Raman spectroscopy and the total carbon measurements.

3.3.2. *Hydrogen production innovative mechanism*

The data given through Table 1, in terms of the composition of the evolved gas during the water splitting process, reveal that different splitting mechanisms were detected through this research review. The following reactions have been reported by [46,47] as the common mechanism of hydrogen production from methanol–water system:

$$MeOH \leftrightarrow H_2CO + H_2$$

$$H_2CO + H_2O \leftrightarrow H_2CO_2 + H_2$$

$$H_2CO_2 \leftrightarrow CO_2 + H_2$$

This mechanism was typically achieved when ZnO–CdS binary semiconductors mixture was used through this work. This can be confirmed through the data displayed in Table 1 since the composition of the obtained gas was 12 and 88 vol% of hydrogen and carbon dioxide, respectively. On the other hand, the introduction of LSCF to the splitting system either in an individual state of combined with the other two semiconductors is revealing an innovative mechanism, due the high percent of hydrogen gas obtained according to Table 1, as follows:

$$MeOH \leftrightarrow H_2CO + H_2$$

$$H_2CO + H_2O \leftrightarrow H_2CO_2 + H_2$$

$$H_2CO_2 \leftrightarrow H_2 + C\downarrow$$

This novel splitting mechanism can be referred to the ability of LSCF which is in a Perovskite structure to scavenge or capture the oxygen atoms which in turn reduce the carbon dioxide into carbon species. The confirmation of carbon deposits formation and the characterization of these carbon species is given in the following section.

3.4. *Carbon species characterization*

At the end of the water splitting process, a visual detection for black species was observed within the splitting system, particularly on the semiconductors utilized during hydrogen production procedures. The semiconductors samples as collected at the end of reaction were then subjected to different analysis in order to examine the formed deposits. Thereafter, the carbon species characterization is introduced through different tools analysis, namely, TEM, surface area, Raman spectroscopy and total carbon content analysis.

3.4.1. *TEM*

The morphology and structures of the LSCF particles after the processing are investigated through the TEM micrographs given in Fig. 8, as next illustrated.

The displayed images, at different spots within the inner structure of LSCF, showed the detection of uniform carbon deposits around the whole sample. By focusing on the details of the carbon species as given through Fig. 8a and b, the given images disclosed the formation of nano-carbon crystals with approximately particles sizes ranged between 10 and 50 nm. The formation of nano-carbon species might be one of the reasons behind improving the surface activity of semiconductors toward water splitting.

3.4.2. *Surface area analysis*

The surface area analysis of both LSCF-CdS and LSCF-ZnO semiconduction binary systems as collected after processing is next given through Figs. 9 and 10. The perovskite-CdS isotherm shape, Fig. 9a, showed a typical Type II instead of Types III and IV of the fresh LSCF and CdS. It also exhibited a typical extending H3 type hysteresis loop that is associated with filling and empting of the mesopores by capillary condensation. This type of loop may indicate preservation of the solid system with the non-rigid aggregates or plate-like particles forming slit-shaped pores [37].

The S_{BET} and the total pore volume of the CdS mixed perovskite increase to 42.07 m^2/g and 0.080 cm^3/g, respectively. The PSD curve (Fig. 9b) of such sample indicates the presence mainly of wider mesopores and pore radii, being centered at 18.5, 28.51, 69.5 Å.

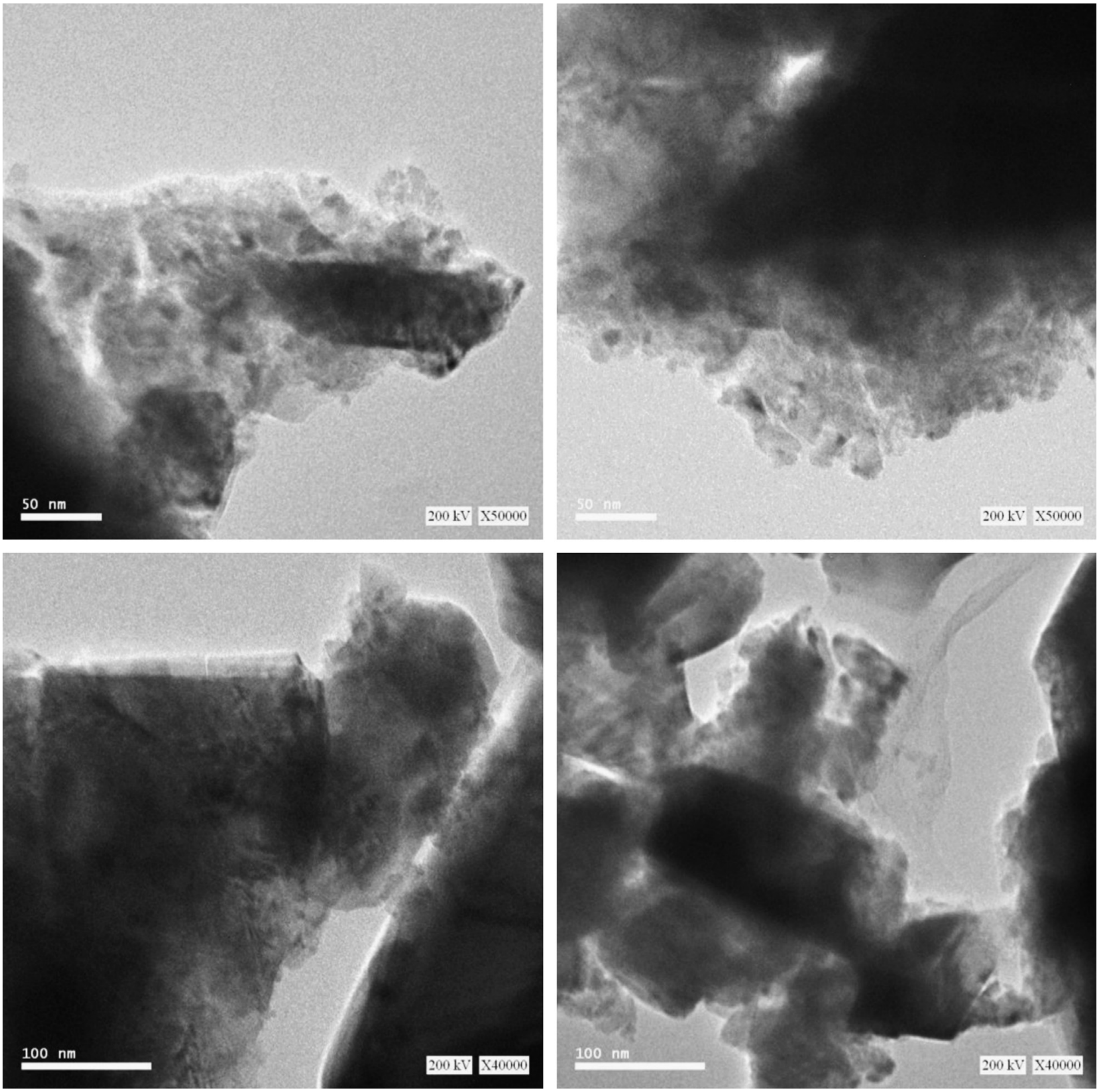

Fig. 8. LSCF particles micrographs at four different spots with the details of carbon species.

For Perovskite-ZnO mixture, the obtained N_2 adsorption-desorption isotherm (Fig. 10a) is of predominantly complex Type IV, characterizing almost stepwise multilayer adsorption on non-uniform surface of mesoporous or microporous materials. The type of hysteresis loop is H4 type, according to IUPAC classification, related probably to narrow slit pores including pores in the micropore region. The obtained solid shows the higher specific surface area of 56.20 m^2/g and total pore volume of 0.074 cm^3/g, as compared with the neat perovskite and ZnO. The obtained solid material is mainly mesoporous, where the mesopores area is 52.24 m^2/g, together with a considerable fraction of micropores with area 3.95 m^2/g. The obtained polymodal PSD curve (Fig. 10b) indicates the presence of mixed micro or narrower mesopores – mesopores systems. The pore radii are centered at 8.08, 10.19, 16.57, 20.15 and 32.33 Å.

Table 2 summarizes the surface parameters of the neat Perovskite samples, ZnO and CdS, as prepared, as well as for the Perovskite mixed samples with CdS or ZnO collected after the completion of the splitting process.

The change in semiconductors isotherms as well as the increase in the surface areas values between the freshly prepared materials, namely, LSCF, ZnO and CdS, and the samples collected after processing can be explained due the formation of the carbon species within the structure of the semiconductors.

3.4.3. Raman spectroscopy analysis

The Raman analysis of as-prepared LSCF, LSCF collected after the splitting process and LSCF-ZnO-CdS triple semiconduction system are given in Fig. 11a, b, and c, respectively.

No carbon indicative peaks, as expected, was detected in Fig. 11a that belongs to the freshly made LSCF since it does not include any carbon components within its chemical formula where it is only composed of La, Sr, Co and Fe metals mixed

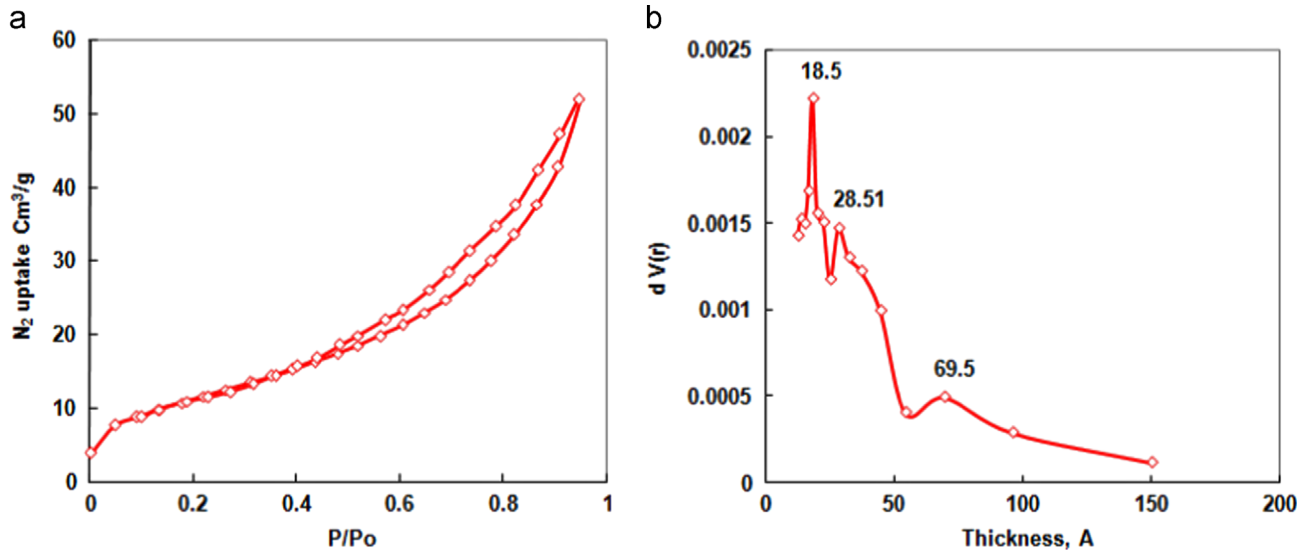

Fig. 9. Perovskite mixed with CdS: (a) N_2 adsorption-desorption isotherm, (b) pore size distribution curve.

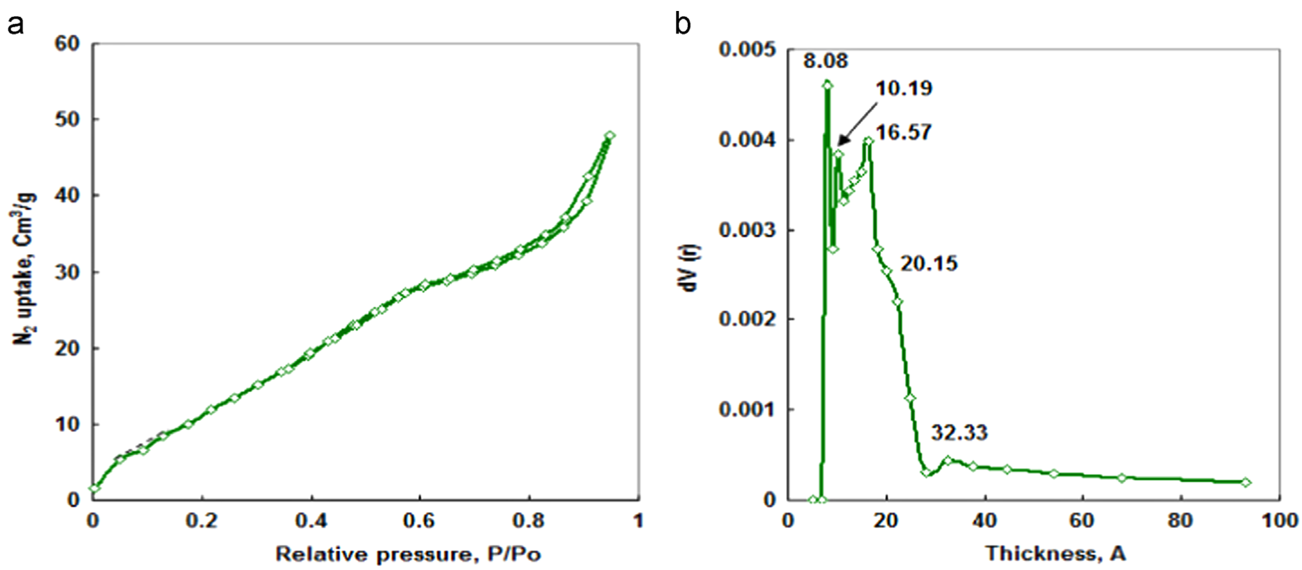

Fig. 10. Perovskite–ZnO sample: (a) N_2 adsorption-desorption isotherm, (b) pore size distribution curve.

Table 2
Surface parameters of Perovskite, ZnO, CdS and Perovskite mixed samples.

Semiconductors	S_{BET} ($m^2 g^{-1}$)	V_P ($cm^3 g^{-1}$)	Average pore radius (nm)
Perovskite	3.44	0.006	3.49
Perovskite+CdS	42.07	0.080	3.81
Perovskite+ZnO	56.20	0.074	2.63
ZnO	18.22	–	–
CdS	24.18	–	–

oxides. On the other hand, both Fig. 11b and c shows indicative peaks for the nano-carbon species at wavenumber between 900 and 1500 cm^{-1} confirming the formation of carbon species within the semiconductors structure. Fig. 11c shows two high intense peaks around 1300 and 1500 cm^{-1} referring to a better activity for the LSCF when mixed with both ZnO and CdS dislike when utilized individually as given in Fig. 11b. The peaks exhibited in Fig. 11c can also refer to the formation of carbon nano-fiber along with the carbon nanoparticles. This can verify the ability of LSCF in reducing CO_2 into carbonaceous materials during the water splitting process.

3.4.4. Total carbon analysis

The total carbon content of the freshly prepared Perovskite [LSCF] and the semiconductors collected after being processed in the water splitting, namely, LSCF and LSCF-CdS-ZnO, are summarized in Table 3.

The data shown above is matched with the TEM, Raman analysis and the surface area analyses and obviously confirming the formation of carbon materials as by-products for the hydrogen evolution process from water. The total carbon analysis also verifies the high activity of LSCF toward the reduction of carbon dioxide into carbon while releasing pure hydrogen.

4. Summary and conclusion

Hydrogen has become a viable compound and attracted much attention these days as a clean energy carrier due to its huge energy content. Nevertheless, the hydrogen-based energy can receive greater interest and importance when it is combined with low production cost via an efficient process that can yield high level of hydrogen. In line with this scope, several investigations

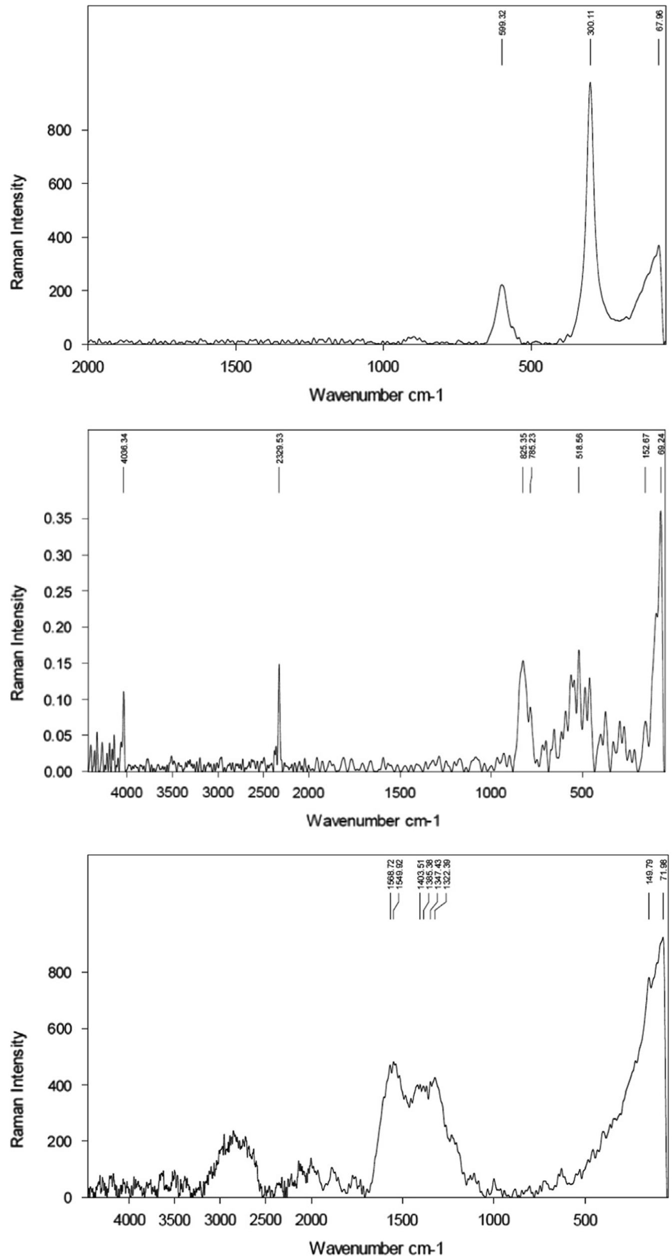

Fig. 11. Raman Spectroscopy analysis of Perovskite samples.

Table 3
Carbon content of neat Perovskite, used Perovskite and Perovskite ternary mixed samples.

Semiconductors	Total Carbon (g/kg)
Perovskite	0.00
Perovskite after processing	31053
Perovskite+ZnO+CdS	285331

and studies were done over the last few decades by many researchers using various kinds of materials as given before in the introduction section of this research/review. The hydrogen yield through their studies is not highly satisfying since a maximum of 3 mmol of hydrogen could be attained.

The team of this work aimed to improve the hydrogen production level via using a novel Perovskite structure, either individually or combined with other oxides, while moving the production cost to the lowest. In practical, three different semiconductors namely mixed oxides of lanthanum, strontium, cobalt and iron as a combined mixture in the following formula ($La_{0.6}Sr_{0.4}Co_{0.2}Fe_{0.8}O_3$), which is known as the Perovskite structure, cadmium sulfide (CdS) and zinc oxide (ZnO) are utilized through this research review. The texture properties and morphology of the prepared LSCF nanoparticles by SEM and TEM show a smooth, nonuniform and highly porous structure even after thermal treatment at 1200 °C. SEM analysis at high magnifications also showed the formation of a metal oxide mixture layer of particles ranging in size from about 1 µm to few hundreds nanometers. N_2 adsorption-desorption results showed that the neat perovskite has a specific surface area of 3.44 m^2/g while the total pore volume and the average pore radius are 0.006 cm^3/g and 3.49 nm, respectively. The surface area analysis of both Perovskite mixed CdS and Perovskite-mixed ZnO semiconduction binary systems showed an increase in S_{BET} which reached to 42.07 and 56.20 m^2/g, respectively. The feasibility of generating hydrogen photoelectrochemically from water/methanol decomposition using either LSCF [Perovskite] individually or combined with ZnO or CdS as well as a ternary mixture of LSCF-CdS-ZnO has been demonstrated. In conclusion, it has been shown that LSCF either utilized alone or mixed with zinc oxide or cadmium sulfide has unique photocatalytic activity for hydrogen production from water in the presence of methanol as a hole scavenger under sunlight visible radiation. The overall activity of hydrogen production was 6.35 mmol/h when LSCF was introduced as an individual semiconductor for the water splitting system. Extraordinary hydrogen yield was obtained particularly 24 and 28 mmol/h when LSCF was coupled with CdS and ZnO, respectively. The combination of Perovskite and the other semiconductors was observed to enhance the photocatalytic properties of these materials in comparison to their activities when utilized individually. The nano-structured semiconductors prepared through this work can be promising candidates in the production of H_2 at the industrial scales. Eventually, an innovative mechanism for the water splitting has been revealed through this work since pure hydrogen was obtained, instead of H_2 and CO_2 mixture, with in situ nano-carbon species. The TEM of the LSCF particles after the processing showed different spots within the inner structure of LSCF and showed the detection of uniform carbon deposits around the whole sample. By focusing on the details of the carbon species, the formation of nano-carbon crystals with approximately particles sizes ranged between 10 and 50 nm was disclosed. The formation of nano-carbon species might be one of the reasons behind improving the surface activity of semiconductors toward water splitting; this is confirmed by Raman spectroscopy and the total carbon measurements.

References

[1] Arai N, Saito N, Nishiyama H, Domen K, Kobayashi H, Sato K, et al. Effects of divalent metal ion (Mg^{2+}, Zn^{2+} and Be^{2+}) doping on photocatalytic activity of ruthenium oxide-loaded gallium nitride for water splitting. Catal Today 2007;129:407–13.

[2] Shen S, Zhao L, Guo L. $Zn_mIn_2S_{3+m}$ (m=1-5, integer): a new series of visible light driven photocatalysts for splitting water to hydrogen. Int J Hydrogen Energ 2010;35:10148–54.

[3] Zhang X, Jing D, Guo L. Effects of anions on the photocatalytic H_2 production performance of hydrothermally synthesized Ni-doped $Cd_{0.1}Zn_{0.9}S$ photocatalysts. Int J Hydrogen Energ 2010;35:7051–7.

[4] Zou Z, Arakawa H. Direct water splitting into H_2 and O_2 under visible lightirradiation with a new series of mixed oxide semiconductor photocatalysts. J Photochem Photobiol 2003;158:145–62.

[5] Hu X, Li G, Yu JC. Design, fabrication, and modification of nanostructuredsemiconductor materials for environmental and energy applications. Langmuir 2010;26:3031–9.

[6] Maeda K. Photocatalytic water splitting using semiconductor particles: history and recent developments. J Photochem Photobiol C: Photochem Rev 2011;12:237–68.

[7] Ni M, Leung MKH, Leung DYC, Sumathy K. A review and recent develop-ments in photocatalytic water-splitting using TiO_2 for hydrogen production. Renew Sustain Energ Rev 2007;11:401–25.
[8] Morales-Torres S, Pastrana-Martinez LM, Figueiredo JL, Faria JL, Silva AMT. Desing of grapheme-based TiO_2 photocatalysts—a review. Environ Sci Pollut Res 2012;19:3676–87.
[9] Morales-Torres S, Pastrana-Martinez LM, Figueiredo JL, Faria JL, Silva AMT. Graphene oxide-P25 photocatalysts for degradation of diphenhy-dramine pharmaceutical and methyl orange dye. Appl Surf Sci, in press, http://dx.doi.org/10.1016/j.apsusc.2012.11.157.
[10] Pérez-Larios A, Gómez R. Hydrogen production using mixed oxides: TiO_2-M (CoO and WO_3). Advances Investigación en Ingeniería 2013;10:27–34.
[11] Tseng IH, Jeffrey CSW. Chemical states of metal-loaded titania in the photo-reduction of CO_2. Catal Today 2004;97:113–9.
[12] Sreethawong S, Suzuki Y, Yoshikawa S. Photocatalytic evolution of hydrogen over mesoporous TiO_2 supported NiO photocatalyst prepared by single step sol–gel process with surfactant template. Int J Hydrogen Energ 2005;30:1053–62.
[13] Erdóelyi A, Raskó J, Kecskés T, Tóth M, Dömök M, Baán K. Hydrogen formation in ethanol reforming on supported noble metal catalysts. Catal Today 2006;116:367–76.
[14] Yoong LS, Chong FK, Dutt BK. Development of copper-doped TiO_2 photo-catalyst for hydrogen production under visible light. Energy 2009;34:1652–61.
[15] César DV, Robertson RF, Resende NS. Characterization of ZnO and TiO_2 catalysts to hydrogen production using thermoprogrammed desorption of methanol. Catal Today 2008;133–135:136–41.
[16] Banerjee AN. The design, fabrication, and photocatalytic utility of nanostruc-tured semiconductors: focus on TiO_2-based nanostructures. Nanotech Sci Appl 2011;4:36–65.
[17] Galindo-Hernández F, Gómez R. Degradation of the herbicide 2,4-dichloro-phenoxyacetic acid over TiO_2–CeO_2 sol–gel photocatalysts: Effect of the annealing temperature on the photoactivity. J Photochem Photobiol A: Chem 2011;217:383–8.
[18] Nakamura I, Negishi N, Kutsuna S, Ihara T, Sugihara S, Takeuch K. Role of oxygen vacancy in the plasma-treated TiO_2 photocatalyst with visible light activity for NO removal. J Mol Catal A: Chem 2000;161:205–12.
[19] Ihara T, Miyoshi M, Iriyama Y, Matsumoto O, Sugihara S. Visible-light-active titanium oxide photocatalyst realized by an oxygen-deficient structure and by nitrogen doping. Appl Catal B Environ 2003;42:403–9.
[20] El Naggar AMA, Nassar IM, Gobara HM. Enhanced hydrogen production from water via a photo-catalyzed reaction using chalcogenide d-element nanopar-ticles induced by UV light. Nanoscale 2013;5:9994–9.
[21] Eng HW, Barnes PW, Auer BM, Woodward PJ. Investigations of the electronic structure ofd^0 transition metal oxides belonging to the perovskite family. Solid State Chem 2003;175:94–109.
[22] Osterloh FE. Inorganic materials as catalysts for photochemical splitting of water. Chem Mater 2008;20:35–54.
[23] Takata T, Furumi Y, Shinohara K, Tanaka A, Hara M, Kondo JN, et al. Photocatalytic decomposition of water on spontaneously hydrated layered perovskites. Chem Mater 1997;9:1063–4.
[24] Schaak RE, Mallouk TE. Perovskites by design: a toolbox of solid-state reactions. Chem Mater 2002;14:1455–71.
[25] Arakawa H, Zou Z, Sayama K, Abe R. Direct water splitting by new oxide semiconductor photocatalyst under visible light irradiation. Pure Appl Chem 2007;79:1917–27.
[26] Zou Z, Ye J, Arakawa H. Role of R in Bi_2RNbO_7 (R=Y, Rare Earth): effect on band structure and photocatalytic properties. J Phys Chem B 2002;106:517–20.
[27] Zou ZG, Arakawa H, Ye JH. Substitution effect of Ta^{5+} by Nb^{5+} on photo-catalytic, photophysical and structural properties of $BiTa_{1-x}Nb_xO_4$ ($0 \le x \le 1.0$). J Mater Res 2002;17:1446–54.
[28] Baykara SZ. Hydrogen production by direct solar thermal decomposition of water, possibilities for improvement of process efficiency. Int J Hydrogen Energ 2004;29:1451–8.
[29] James EF. Thermochemical hydrogen production: past and present. Int J Hydrogen Energ 2001;26:185–90.
[30] Grasse W, Becker M, Kuhn P, Tyner C. EA Solar PACES Annual Report, Deutsche Forschungsanstalt fur Luft- und Raumfahrt e.V., Koln; 1995, P. 62-63.
[31] Steinfeld A, Kuhn P, Reller A, Palumbo R, Murray J, Tamaura Y. Solar-processed metals as clean energy carriers and watersplitters. Germany: Hydrogen Energy Progress XI. DECHEMA; 1996; 601–9.
[32] Nassar IM, Osipova VV, Safiullin G, Lobkov V, Galyametdinov Yu. Preparation of II-VI semiconductors nanoparticles and investigation of their photo physical properties. Int J Green Nanotech 2011;1:22–36.
[33] Akay G, Al-Harrasi W, El-Naggar AMA, Mohamed A, Zhang K. Integrated intensified BioRefinery for gas-to-liquid conversion [GB2013/050125], UK Patent, No: **WO2013108047 A2**; 2013.
[34] El Naggar AMA, Akay G. Intensified nano-structured Perovskite based catalytic membranes for high temperature oxygen separation, American Institute of Chemical Engineers Conference (AIChE), October, Pittsburgh; Pennsylvania; USA; 2011.
[35] El Naggar AMA, Akay G. Novel intensified catalytic nano-structured nickel-zirconia supported palladium based membrane for high temperature hydro-gen production from biomass generated syngas. Int J Hydrogen Energ 2013;38:6618–32.
[36] El Naggar AMA, Kazak C, Akay G, Connell M, Kolb G. Composite intensified catalytic membrane for high temperature hydrogen separation. American Institute of Chemical Engineers Conference (AIChE), November; Topical 5: Nano-materials for Energy Applications, Nano-materials for Energy Produc-tion and Fuel Cells II, Salt Lake City; Utah; USA; 2010.
[37] Sing KS, Everett DH, Haul RA, Moscou L, Pierotti RA. Reporting physisorption data for gas / solid systems with special reference to the determination of surface area and porosity. Pure Appl Chem 1985;57:603–19.
[38] Ni Meng, Michael KH, Dennis YC, Sumathy K. A review and recent develop-ments in photocatalytic water-splitting using TiO_2 for hydrogen production. Renew Sustain Energy Rev 2007;11:401–25.
[39] Liu L, Li P, Adisak B, Ouyang S, Umezawa N, Ye J, et al. Gold photosensitized $SrTiO_3$ for visible-light water oxidation induced by Au interband transitions. J Mater Chem A 2014;2:9875–82.
[40] Tijare SN, Rayalu SS, Khaty NT, Labhsetwar KN. Photocatalytic hydrogen generation by ethanol assisted water splitting reaction using mixed oxide of Ba and Mn. Int J Know Eng 2012;3:127–9.
[41] Jang JS, Borse PH, Lee JS, Lim KT, Jung O-S, Jeong ED, et al. Photocatalytic hydrogen production in water-methanol mixture over iron-doped $CaTiO_3$. Bull Korean Chem Soc 2011;32:95–9.
[42] Choi J, Ryu SY, Balcerski W, Leeb TK, Hoffmann MR. Photocatalytic production of hydrogen on Ni/NiO/$KNbO_3$/CdS nanocomposites using visible light. J Mater Chem 2008;18:2371–8.
[43] Pérez-Larios A, Lopez R, Hernández-Gordillo A, Tzompantzi F, Gómez R, Torres-Guerra LM. Improved hydrogen production from water splitting using TiO2–ZnO mixed oxides photocatalysts. Fuel 2102; 100: 139–43.
[44] Kudo A. Photocatalyst materials for water splitting. Catal Survey Asia 2003;7:31–8.
[45] Ye J, Zou Z, Arakawa H, Oshikiri M, Shimoda M, Matsushita A, et al. Correlation of crystal and electronic structures with photophysical properties of water splitting photocatalysts $InMO_4$ ($M=V^{5+}$, Nb^{5+}, Ta^{5+}). J Photochem Photobiol 2002;148:79–83.
[46] Kawai T, Sakata T. Photocatalytic hydrogen production from liquid methanol and water. J Chem Soc. Chem Commun 1980;15:694–5.
[47] Chen J, Ollis DF, Rulken WH, Bruning H. Photocatalyzed oxidation of alcohols and organochlorides in the presence of native TiO_2 and metallized TiO_2 suspensions. Part (II): Photocatalytic mechanisms. J Water Res 1999;33:669–76.